ResearchGate

See discussions, stats, and author profiles for this publication at: https://www.researchgate.net/publication/361098132

An experimental comparison of innovative 3D-printed acoustic metamaterial designs

Presentation · November 2019

CITATIONS
0

READS
230

4 authors, including:

Ferguson Hamilton Tobins
University of Abuja
22 PUBLICATIONS **45** CITATIONS

SEE PROFILE

All content following this page was uploaded by Ferguson Hamilton Tobins on 05 June 2022.

The user has requested enhancement of the downloaded file.

An experimental comparison of innovative 3D-printed acoustic metamaterial designs

Mathis GROSSO[a,*], Matthieu PROFFIT[a], Ferguson TOBINS[a], Colin BETTINI[a]

[a]*School of Engineering, Trinity College Dublin, University of Dublin, Dublin, D02PN40, Ireland*

Abstract

This paper concerns the use of 3D-printing to manufacture acoustic meta-materials. From the literature, three new designs have been derived and adapted: a Helmholtz resonator coupled with quarter length tube resonators, a semi-closed air cavity followed by a micro-helix unit and a split-ring neck resonator. The Helmholtz cell is analytically designed and the micro-helix modelling strategy is presented. The transfer function method also referred to the two microphones tube impedance method is used to assess the sound absorption coefficient of each design, according to the standards ISO10534-2:2001 and GB/T18696.2-2002. The experimental acoustic performances are compared and discussed over the frequency range [500; 3500] Hz. The three solutions achieve singular acoustic behaviours that can solve specific applications in different industries. The Helmholtz/quarter length tubes and the split ring neck resonators lead respectively to a spectrum with several or unique local resonant frequencies. The helical geometry coupled to an air cavity affects the entire spectrum due to wave compression and expansion causing thermal losses.

Keywords: Acoustic metamaterials, Sound absorption, Design comparison, 3D-printing FDM/MSLA, Helmholtz resonator, Quarter length resonator, Micro-Helix, Spiral, Split-ring neck resonator

1. Introduction

Meta-materials are materials that can exhibit new properties feasible from a physical point of view but that can't be found in classical materials and may seem paradoxical at first look. They present unusual properties such as negative (or near-zero) values of effective permeability, effective permittivity, or density over a certain narrow frequency band [1]. These metamaterials are fabricated structures or composites generated artificially using inclusions or inhomogeneities.
Their properties have been predicted and experimented in several fields such as electromagnetism, optics, acoustic and structural mechanics and turn out to be useful for many applications. If the goal of meta-material is mainly to control waves properties, they have also found many applications such as weight, size, and performance enhancement through wave attenuation or transmission.
The apparition of these artificial materials begun at the end of the 19^{th} century by the research of Jadagis Chunder Bose [2] who worked on twisted elements known today as chiral metamaterials. From the late 40s to 60s, lightweight microwave antenna lenses have been investigated by Winston e. kock [3]. Later on, the research has been focused on these artificial chiral metamaterials used for microwave radar absorbers [1],[4],[5],[6]. If the very first research were focused on electromagnetic metamaterials, acoustic metamaterials are now actively studied, many types of them exist that can be classified as shown below :

- passive metamaterials: they do not supply energy to the wave and are not actively controlled by an external source
- active metamaterials: they are either controlled by an external source or require energy input to work

Metamaterials can also be classified according to their index and density :

- Simple negative materials (SNG) which have a negative refraction value over a range of frequencies.
- Double negative materials (DNG) which show a negative density and refraction value. Both simple and double negatives involve length and dimensions much smaller than the wavelength considered.

As their electromagnetic counterparts, they show unusual but similar wave physics (presented previously) but this time in term of sound propagation in air or water, bulk or surface elastic waves in solids, or other types of mechanical wave motion.[7]. From the equation of propagation of scalar pressure waves inside a homogeneous linear fluid (see Eq.1), we can see which physical constants are involved for acoustic.

$$\nabla^2 P(r) - \frac{\rho}{B}\frac{\partial^2 P(r)}{\partial t^2} = 0 \tag{1}$$

Where P is the acoustic pressure, ρ and B stand respectively for the mass density and the bulk modulus. Standard materials have both constants positive. As bulk modulus and density are the two main physical constants that determine a medium's acoustic behaviour, researchers are creating metamaterials with at least one of these parameters being negative.

The sound attenuation or transmission loss of a wall is proportional to $\rho d\omega$, corresponding respectively to the mass density, the thickness and the frequency. Low frequencies are thus

*Corresponding author. Email address: grossom@tcd.ie

easily transmitted. Locally resonant AMMs are the most common passive AMMs. They rely on the frequency dispersion, delayed by the structure inertia, that can be leveraged to generate destructive interference and so anomalous properties. In their work in 2000, Liu et al [8], were inspired by electromagnetic metamaterials to create an unprecedented Locally Resonant Sonic Materials (LRSMs), the first AMMs. The idea is to create an artificial structure that exhibit negative elastic constants at certain relevant sonic frequencies, like their electromagnetic counterpart. To reach this goal, their meta-material is composed of a lattice of the locally resonant structural unit. It uses lead balls, coated with silicon, their size and shape define the frequency ranges over which the material exhibit effective negative constants. Recent studies developed new technologies that show identical properties. The resonator can be spring-mass systems, acoustic membranes or pillar resonators [9].

Another way leverages the compression extension of the air. Small cavities are manufactured to become strong resonators (Helmholtz resonance). During oscillation, the gas within the volume of the resonator is alternately compressed and expanded at very low magnitudes. By adjusting the shape of the neck and chamber volume, it is possible to dampen noise over a specific frequency domain. It is considered as a negative bulk modulus, creating high sound absorption [10].

The combination of the two previous technologies can generate negative mass density and bulk modulus for the same range of frequencies. The structure combine air resonators and membranes. These double negative AMMs has a negative index of refraction, very useful in cloaking, lensing...
The power of locally resonant AMMs is based on a dynamic phenomenon of resonance, and so, is available only on a specific bandwidth. Dai *et al.* [11] studied the properties of LRSMs and found that in some structure, the main acoustic properties were determined only by the resonators, independent of their spatial arrangement. In particular, the acoustic properties of a single resonator resemble that of an assembly of resonators. According to them, when the lateral coupling of resonators was properly designed, it could generate multi-mode resonances, leading to multiple stopbands.

Non-resonant, or space coiling AMMs present a structure of sub-wavelength curled channels. Besides a larger bandwidth, they don't exhibit a high absorption at resonant peak but anomalous properties as negative refraction of sound. It is also a relevant way to slow down the acoustic waves.

Another interesting metamaterial's geometry has been manufactured by Gao *et al.*: a lightweight micro-helix metamaterial [12] that shows great sound absorption properties thanks to the friction between the helix vestibule and the air. Other technologies showing great absorption as acoustic black hole (ABH) effect producing drastic wave compression and energy trapping in thin-walled structures has been performed using 3D printers [13].

As 3D printing is developing, it is possible to print structures with finer details at a decreasing cost. As metamaterials often have a very complex structure with cavities and fine features, traditional machining is not appropriate to manufacture them. Furthermore, 3D printing allows rapid prototyping which is very useful for research applications. For example, the Stereolithography (SLA) technique allows a very good precision. The SLA printers used to manufacture the samples presented in this study have a resolution of 80μm cost less than 500μm.

If FDM and MSLA are interesting technology in term of price quality-ratio, other precise technologies as PolyJet technology are used to design samples with high sound absorption [14]. Cellular thin-walled periodic structures with links between the cells can be synthesized by photopolymer material using this additive technology similar to ink-jet technology.

Helmholtz resonators, helix shape metamaterials and sub-wavelength absorbing cavities have previously been studied in the literature and are known to exhibit a wide behaviour. However, they have not, to the writer's knowledge been compared yet. Every experiment has been conducted in different laboratories, with different test rigs, protocols and the samples are manufactured with widely different techniques and materials. This study aims at comparing their absorbing properties by reducing the number of factors by which the experiments differ. This will provide a consistent benchmark to compare those techniques and maybe help choosing the appropriate solution for a specific application.

2. Design and manufacturing

The first design is based on the notions of Helmholtz and tube length resonators. The knowledge about these two previous devices has been widely developed and their behaviour can be found accurately by an analytical approach. They can absorb a signal at a local frequency which turns out to be useful to stop a resonant frequency while leaving the spectrum unchanged. By coupling a Helmholtz resonator characterised by a certain volume and a neck length with a circular array of tubes with different lengths, it was possible to stop particular frequencies determined by the previous geometric parameters (see Fig.1.a). A sufficient amount of cells were grouped to observe an overall absorption response (see Fig.1.b).

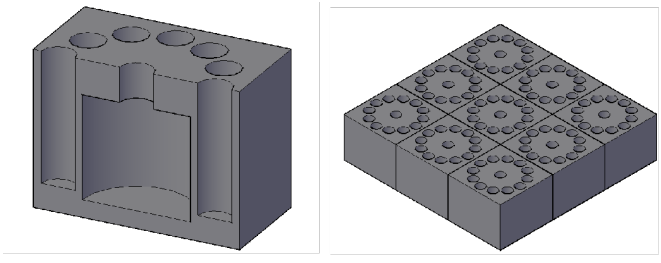

Figure 1: Helmholtz/Quarter-length tube cells metamaterial: (a) Multiple cells array, (b) Cross section of one unit cell

The second metamaterial design was derived from analytical analysis of Yuan *et.al* [15] (see Fig.2). The device is an assembly looking like a box. An inner neck and an outer neck are connected by a gap. The inner neck is directly linked to the acoustic inlet. The other side of the outer neck is opened

to a cylindrical cavity through another outer gap. Yuan *et.al* predicted a response close to a perfect Helmholtz resonator *i.e.* a peak at a particular frequency (see Fig.A.14,to visualise the spectrum). The ring showed theoretically an absorption of 1 while the equivalent Helmholtz resonator only reached 0.6 at 200 Hz. This geometry needs to be tested to validate the theoretical improvements.

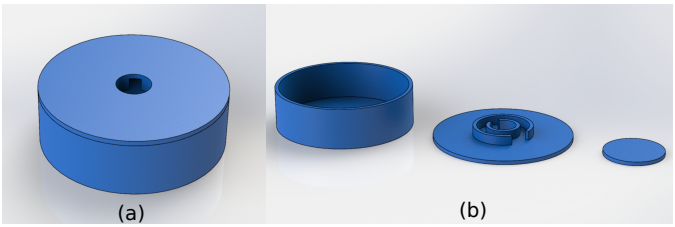

Figure 2: Split-ring neck design: (a)Assembly, (b) Exploded view

The last metamaterial is a combination of an air cavity followed by an array of helices (see Fig.3). Compared to the two previous design, it is slightly more cumbersome as the device grouped two consecutive geometries. The wave is entering the first cavity through a fence like surface (see Fig.3.a). That allows a part of the entering wave to be reflected several times through the cavity before exiting it. Moreover, another part of the wave kept in the cavity is dissipated through the helical hole matrix (see Fig.3.b). The sound absorption capacity of helix shape metamaterial has been investigated recently by Gao *et al.* [12] and turned out to be promising. Gao *et al.* used the opposite geometry *i.e.* an in-line array of solid micro-helices. However, some physical effect are common:

- The helical shape is modifying the wave front which creates wave interactions.
- The wave is subject to multiple compression and expansion through the spiral cavities which dissipates some energy through viscous effect.

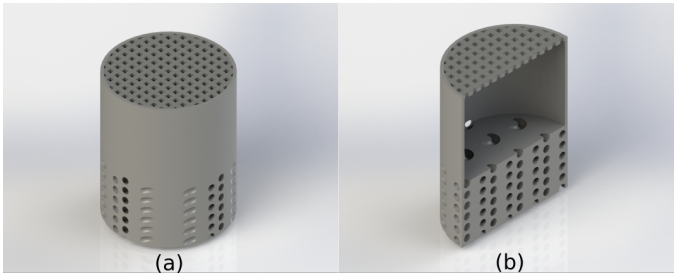

Figure 3: Micro-helix cavity design printed as an acoustic cylinder: (a) Overall view, (b) Cross section

If the material and the process can have some effect on the sound absorption [16], the order of magnitude and absorption profile should be consistent independently of the material. The processes were then chosen to give the fastest usable results while keeping good accuracy.

First, the Helmholtz/Quarter length cells, as well as the split-ring neck resonator, were manufactured using Fused Deposition Modeling (FDM). Their simple geometry mainly characterised by cylindrical and plane surfaces with low wall angles led to a good accuracy using this process.

Finally, the micro-helix showed the most complex geometry. The 3D-printed FDM could be suitable for this purpose. However, it provides a lower accuracy than the previous geometries and would ask a more complex printer calibration due to its complexity. Mask Stereolithography (MSLA) is giving better surface roughness. The angle at which the helix needs to be printed is relatively high. For an angle close to 45^o between the shape and the 3D-printer bed the result will be coarse. Above this value the part is unusable. Using MSLA allows to print very thin layers while avoiding any layer separation. This process suited well our purpose. Is is also easier to undertake as the mean accuracy is higher with default printing parameters.

3. Analytical approaches and performance expectations

3.1. Analytical performance of Helmholtz/Quarter length tube cells

A Helmholtz resonator behave as a mass-spring system. The resonant frequency f_0, which produces a high absorption, is given in the following equation 2:

$$f_0 = \frac{c}{2\pi}\sqrt{\frac{S_h}{l_h * V_h}} \tag{2}$$

where S_h is the area of the the Helmholtz resonator opening, V_h the volume of its cavity and l_h is the actual neck length. Finally c corresponds to the speed of sound in the air and is approximately equal to $343\,\mathrm{m.s^{-1}}$ in standard conditions. The design of the resonator is resumed in table 1.

Table 1: Geometric parameter of the Helmholtz metamaterial

Parameter	l_h	S_h	V_h
Value	10 mm	78.54 mm^2	23500 mm^3

The expected resonant frequency is around $f_0 \approx 998Hz$.
In the design, the resonator is implemented with a set of quarter wavelength resonator in parallel to cover a wider range of frequency. A quarter wavelength resonator has a resonant frequency as expressed in equation 3:

$$f_0 = \frac{c}{\lambda} = \frac{c}{4L_q}\ [17] \tag{3}$$

where L_q is the length of the quarter length tube and c is the speed of sound in the air ($\approx$ 343 $\mathrm{m.s^{-1}}$). 12 tubes are implemented, in 6 pairs of twins. The length are set to cover the range between the 2000 and 2500Hz. It is resumed in table 2.

Table 2: Geometric parameter of quarter length tube

Tube	1	2	3	4	5	6
L_q (mm)	42.9	40.8	39.0	37.3	35.7	34.3
f_0 (Hz)	2000	2100	2200	2300	2400	2500

3.2. Micro-helix cavity expected performance

The sound absorption characteristics of an array of helices is dependent of the air particles friction. Air will be kept inside the vestibule and will act as a damper. The compression of the air will vary depending on the height of the array. Gao *et al.* [12] work showed promising performance in term of sound absorption. By adding an air chamber before the helix array, the sound absorption may be enhanced as the wave entering the helices will have a lower energy to dissipate. Every frequencies should be affected as the helical geometry kept the air inside its geometry and is not based on destructive interference. However a range of frequencies should be more affected than the rest of the spectrum as it has been shown by Gao *et al.* [12] (Fig.A.16).

4. Numerical Modelling Strategy

The Helmholtz quarter length tube devices, as well as the split ring neck responses, can be developed analytically. However, a helical/air cavity theory is much more complicated to perform. Gao *et al.* used the "Capillary tube" described through equation 4. Helix vestibule structure is analogous to “Capillary tube” model. This model is taking into account the heat conduction inside and outside the tube. In capillary tubes, the sparse and dense process of a sound wave can be treated as an isothermal process instead of an adiabatic process. The speed of sound is then expressed depending on the specific heat of air γ.

$$\begin{cases} \alpha = \dfrac{4}{c_0 D}\sqrt{\dfrac{\gamma\eta\omega}{\rho_0}} \\ c = \dfrac{c_0}{\sqrt{\gamma}} \end{cases} \tag{4}$$

where $\gamma = 1.4c_0$ is specific heat ratio of air, η is shear viscosity coefficient of air, ω the angular wave frequency, $rho_0 = 1.29\text{kg/m}^3$ is air density and D the diameter of the helices (in this case the diameter of the helical holes).

This model constitutes already an approximation of the spiral cavity part. As two consecutive cavities are much more complicated to model, a numerical study was performed. The meshing strategy over the part is later presented. Some areas where the energy is mainly dissipated needs certain requirements such as refinements to be able to quantify accurately the thermal losses a showing very low magnitude.

In order to perform effective CFD simulations of the geometries presented above, a good mesh of the system is required. A meshing strategy will be presented in order to study the micro-helix cavity resonator. The geometry presents many intricate details and self-similarities, if we wanted to mesh the full cavity (see Fig.4.a), the computational time would be very high: we can make a few assumptions that allow us to reduce the region of interest to a single helix (see Fig.4.b). If we study the system with a planar normal incident wave, the cavity sidewalls would have a negligible effect compared to the helix’s walls and the resonance phenomenon in the cavity. This is why we considered that boundary effects could be neglected and instead of considering an array of circular cavities, we could assimilate

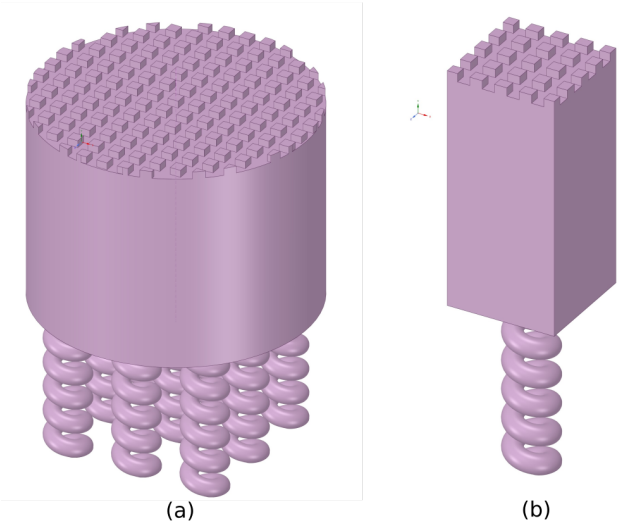

Figure 4: Geometry derived from the assembly. Numerical modelling is applied on the air inside the device : (a) Overall cylinder for tube impedance method, (b) Elementary cell for simulation

that to an infinitely large single cavity with micro-helix. Therefore we can simplify this system to the study of a single helix + resonator as shown in figure 4.b with symmetry boundary conditions on each wall. This assumption allows us to reduce the region of interest to less than a ninth of the original cavity. Furthermore, the results we will obtain could be more easily compared to later studies as they won’t depend on boundary effects.

As in micro-helix array, the sound is absorbed by friction in the boundaries [12], the region of interest is close from the walls, this is why we enhanced the mesh precision around them as shown in figure 5.a.

The air inlet is also a region of interest as it would only allow a fraction of the incident wave to enter or leave the cavity, as the entrance is rather small, we can expect non-negligible air friction around that area. Again, we meshed carefully the inlet as shown in figure 5.b, to take into account the boundary layer at each pore.

Finally, an overall view of the mesh in presented in figure 5.c, this mesh is made of 1,333,190 nodes and 307,346 elements.

5. Experimental Method

The two microphones impedance tube method also refers as transfer function method [18] was used to determine the acoustic sound absorption coefficient α. Several measures were taken for each sample to find a standard deviation and eliminate abnormalities. The physical phenomena involved in the sound absorption were thus accurately analysed.

This method uses a speaker to generate plane waves on a range of frequencies (see Fig.6). Then the sound pressure is measured using two microphone close to the sample. From the two microphone responses, the sound propagation function can be retrieved and absorption can be deduced. This method

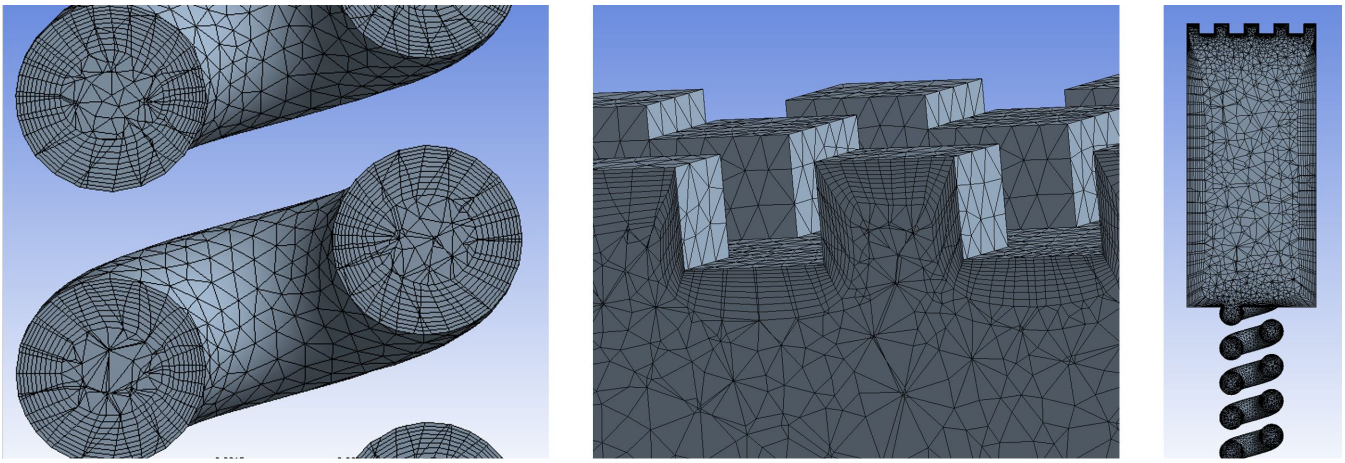

Figure 5: (a) Meshing inside the micro-helix, (b) Cut view of the air inlet, each pore's boundary layer is meshed carefully (c) Cut view of the system's mesh

is following the standards *ISO10534-2:2001* and *GB/T18696.2-2002*.

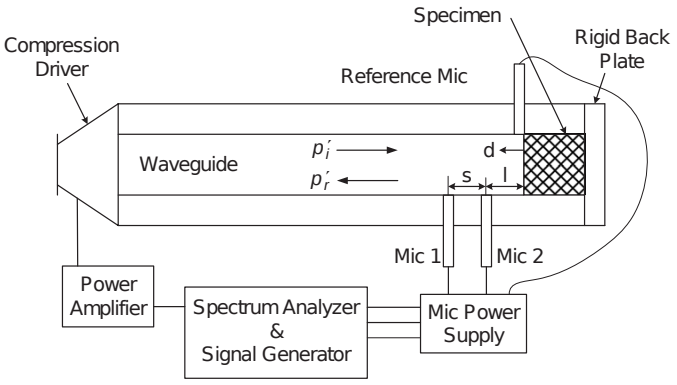

Figure 6: Two microphones impedance tube method/Transfer function method [18], schematic from Schultz *et al.* [19]

Other method using only one sensor like the standing wave method are less accurate and convenient. Standing wave method uses only the maximum and minimum pressure measured with a movable microphone in a standing wave tube to determine the absorption. It requires much more measurements time and introduce a higher uncertainty as the microphone needs to be move and the pressure level has to be found by the experimenter manually.

Based on the plane wave assumption, the sound field inside the wave guide can be described using equation 5).

$$p = Re(P_i(e^{j(\omega t+kd)} + Re^{j(\omega t-kd)})) \tag{5}$$

The term $e^{j(\omega t+kd)}$ represents the incident waves while the $e^{j(\omega t-kd)}$ term represents the reflected waves. d is the axial distance from the sample surface, k is the wave number defined by the equation 6:

$$k = \frac{\omega}{c_0} \tag{6}$$

with $c_0 = \sqrt{\gamma R_{gas} T}$ and corresponds to the isentropic speed of sound depending on γ, the ratio of specific heats, T, the absolute temperature and R_{gas} is the ideal gas constant. k is real when the dissipation and the dispersion are not taken into account. The previous formula 6 is suited for an ideal gas. This assumption is made for this study. P_i represents the complex pressure amplitude of the incident wave and ω is the angular frequency. $Re()$ and $Im()$ signified respectively the real part and the imaginary part of a complex number. Finally, R is the complex reflection coefficient which needs to be determined to deduce the acoustic absorption α.

The measure of the pressure at the two microphones positioned at the distances $d = l$ and $d = l + s$ from the sample allows to deduce two equations (see Eq.7).

$$\begin{cases} p(d = l) = Re(P_i(e^{j(\omega t+kl)} + Re^{j(\omega t-kl)})) \\ p(d = l + s) = Re(P_i(e^{j(\omega t+k(l+s))} + Re^{j(\omega t-k(l+s))})) \end{cases} \tag{7}$$

s corresponds to the spacing between the two microphones and l is the distance between the sample and the closest microphone (here microphone 2 in Fig.6).

From the two previous equations and knowing the incident wave applied through a speaker, the complex reflection coefficient R can be solved through equation 8.

$$R = \frac{\hat{H} - \hat{H}_i}{\hat{H}_r - \hat{H}} e^{2jk(I+d)} = \frac{\hat{H} - e^{-jks}}{e^{jks} - \hat{H}} e^{2jk(I+d)} \tag{8}$$

$\hat{H}_i$ and $\hat{H}_r$ are respectively the transfer functions for the incident and the reflected wave alone. $\hat{H} = E[\hat{G}_{12}/\hat{G}_{11}]$ corresponds to the estimated frequency response function between the two microphones. In others words, $\hat{H}$ is the transfer function from microphone position one to two. $E[]$ is the expectation operator. $\hat{G}_{12}$ is the estimated cross spectral density, $\hat{G}_{11}$ is the estimated auto-spectral density.

As R is a complex number both real and imaginary parts (respectively R_{Re} and R_{Im}) can be split into a system of two equations and solved as follows (see Eq.9).

$$\begin{bmatrix} R_{Re} \\ R_{Im} \end{bmatrix} = \begin{bmatrix} \frac{2\hat{H_{Re}}cos(k(2l+s)) - cos(2kl) - (\hat{H_{Re}}^2 + \hat{H_{Im}}^2)cos(2k(l+s))}{1 + \hat{H_{Re}}^2 + \hat{H_{Im}}^2 - 2\hat{H_{Re}}cos(ks) - 2\hat{H_{Im}}sin(ks)} \\ \frac{2\hat{H_{Re}}sin(k(2l+s)) - sin(2kl) - (\hat{H_{Re}}^2 + \hat{H_{Im}}^2)sin(2k(l+s))}{1 + \hat{H_{Re}}^2 + \hat{H_{Im}}^2 - 2\hat{H_{Re}}cos(ks) - 2\hat{H_{Im}}sin(ks)} \end{bmatrix} \tag{9}$$

Finally, the absorption coefficient α can be computed from the complex reflection coefficient R as it shown in equation 10. The normalised specific acoustic impedance representing the ratio of the specific medium impedance to the sample impedance can also be derived from R and expressed depending on α.

$$\begin{cases} \alpha = 1 - \|R\|^2 = 1 - R_{Re}^2 - R_{Im}^2 \\ \xi = \dfrac{1+R}{1-R} = \left[\dfrac{1 - R_{Re}^2 - R_{Im}^2}{1 - R_{Re}^2 + R_{Im}^2}\right] + j\left[\dfrac{2R_{Im}}{1 - R_{Re}^2 - R_{Im}^2}\right] = \left[\dfrac{\alpha}{\alpha + 2R_{Im}^2}\right] + j\left[\dfrac{2R_{Im}}{\alpha + 2R_{Im}^2}\right] \end{cases} \tag{10}$$

The considered experimental plan is exposed in table 3.

Table 3: Experimental plan

Factor	Number
Number of design	3
Measurement per configuration	3
Total measurements	9

6. Results

Three measurements were undertaken for each geometry which lead to 9 measurements in total.
The acoustic resonators designs are evaluated over a frequency range from 500 to 3500 Hz. The error is based on the standard deviation over the three measurements.

6.1. Helmoltz/Quarter length tube cells

The first design based on the combination of the Helmholtz resonator and quarter length resonator is showing several distinct regions in its absorption response (see Fig.7).

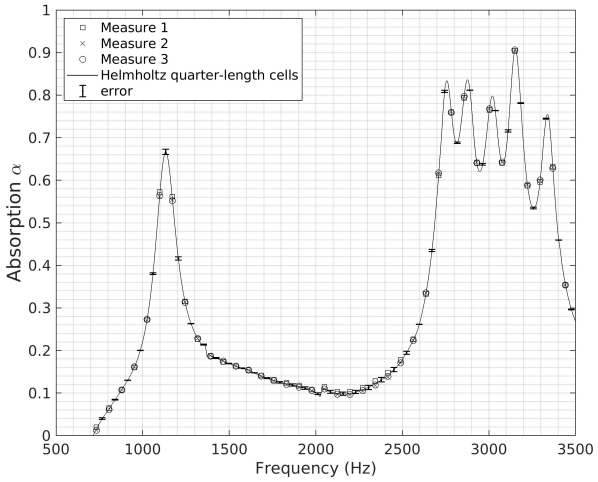

Figure 7: Absorption of the Helmholtz/Quarter-length tube cells over the frequency range [500,3500] Hz. (Errors and measures are sampled and alternated over the mean curve for a better visualisation)

A first peak of absorption around 1200 Hz is reaching a value of $\alpha = 0.7$. Then a larger set of peaks between 2700 and 3300 Hz is visible. The absorption reach locally 0.9 but the region showed an average absorption close to 0.7. Finally between the two previous regions, the sound absorption fluctuates around smaller values mainly localised between 0.1 and 0.3.

6.2. Micro helix cavity

Contrary to the Helmoltz/Quarter length tube cells, the micro helix array combined to the air chamber is showing a smoother characteristic absorption over the same frequency range (see Fig.8).

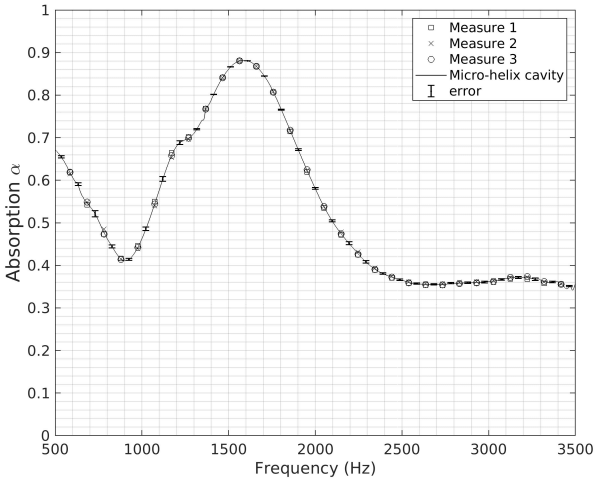

Figure 8: Absorption of the micro-helix cavity design over the frequency range [500,3500] Hz (Errors and measures are sampled and alternated over the mean curve for a better visualisation)

The minimum absorption value over the range of frequency is close to 0.4 which is relatively high. A wide range between 1000 and 2300 Hz is characterised by a good average absorption around 0.75. This region looking like a parabola shape shows a maximum value higher than 0.9 near 1600 Hz. In the lower frequencies, the absorption is characterised by a minimum at 900 Hz. The absorption between 500 Hz and this later minimum shows a decreasing tendency. Finally a plateau seems settled in the higher frequencies.

6.3. Split-ring neck resonator

Split-ring neck resonator response is much more localised than the two previous designs. The response is showing a huge peak around a particular frequency $f = 1800$ Hz (see Fig.9). Around this frequency, the absorption reaches 0.95. From 800 to 1800 Hz the absorption is increasing from 0 to 0.1 as a power law. After the peak, the absorption is decreasing to 0 close to 2750 Hz to finally increasing again to 0.1 at 3500 Hz following a parabola like shape.

7. Discussion

7.1. Comparison with analytical predictions of the Helmoltz/Quarter length tube cell

The analytical prediction can be compared to the experiments for the Helmoltz/Quarter length tube cells. The experimental results are shown figure 7.

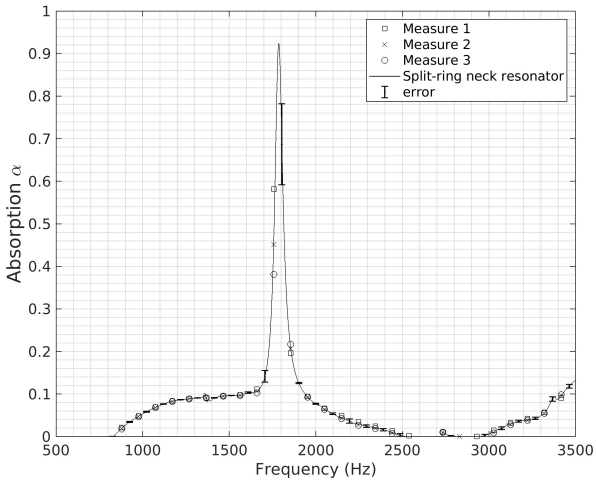

Figure 9: Absorption of the : split-ring neck design over the frequency range [500,3500] Hz (Errors and measures are sampled and alternated over the mean curve for a better visualisation)

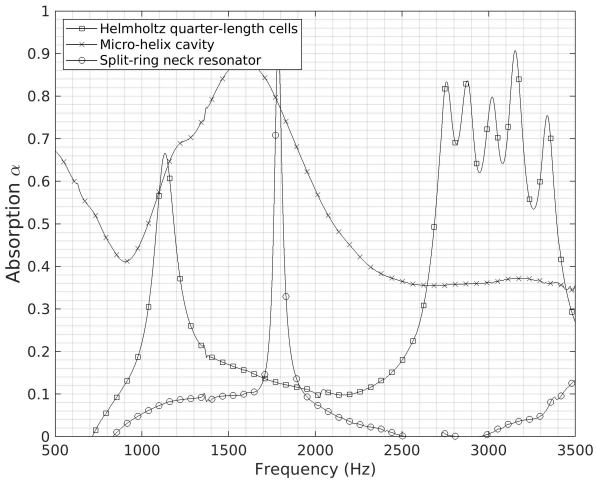

Figure 10: Absorption of the three designs over the frequency range [500,3500] Hz

The effect of the Helmholtz resonator is easily identified. A high absorbance peak stands alone at 1133Hz. It is slightly more than the value of 998Hz from the theory.

The quarter tube length experimental resonant frequencies are also moved to higher frequencies. The range of absorption is between 2754Hz and 3337Hz (first and last peak, against an expectation around 2000-2500Hz). One can observed that the range is also distorted, as it now coverts 600Hz against 500Hz. The point of interest is only 5 absorption peaks are visible over this range, while 6 different quarter length tubes have been designed. Two pairs of tubes may absorb frequency close to 3154Hz as the experiment shows a high absorption peak at this frequency compared to the other peaks.

7.2. Comparison of designs performance

The three different designs shows various absorption over the same frequency range. The three average value obtained are summarised in Fig.10.

In term of mean absorption value, we can see that the micro-helix array coupled with an air chamber performs well. It can be useful in some general noise reduction for human ear health. On the other hand, the Split-ring neck resonator and the Helmholtz modified cells are locally sound absorbing, so they need to be tuned for a specific application. With a correct design, such system could a specific range or individual frequency during communication or in identified resonant system. The predictions of Yuan *et al* are confirmed by the experiments: the Split-ring neck resonator performs a better attenuation, close to 1, than the Helmholtz unit [15].

The compactness of a layer of metamaterial is a relevant factor for the performance assessment. While the Helmholtz resonator and the micro helix cavity have a respective height of 45mm and 49mm, the split-ring neck resonator is only 12mm-high. It makes it an ideal choice for some industries as aeronautic where the space is limited.

7.3. Uncertainty

To validate the sound absorption characteristic over the range, it is necessary to evaluate the standard deviation over the frequency range based on the three measurements realised for each sample. The uncertainty has been sampled on each figures to a certain number of points (see Fig.7,8 and 9).

As a reminder, the samples have been manufactured using 3D printing technologies (FDM and MSLA). These manufacturing processes are not neutral. The material's choice, the printer's accuracy and setup or even the design itself, have an impact on the final structure properties [16]. Some artefacts as the roughness or deformed shapes induced by the process will directly make the results diverge from numerical expectations. If the 3D-printer precision has increased nowadays, the structures are often relatively small because the scale is smaller than the wavelength studied. Printed geometries needs thus to be investigated further in terms of process influence before concluding. To identify a dependency of the results on the processes, further samples have been printed and tested for the most promising design *i.e.* the micro helix array. The tendency were validated and turns out to be mainly independent of the process parameters.

8. Conclusions

Three new metamaterials have been investigated to produce new acoustic behaviours. The Helmholtz resonator acts as a resonant spring-mass system, coupled with quarter length tube based on destructive interference. Split-ring neck design uses a membrane/cavity phenomenon. The last system is composed of a semi-open cavity with helix-holes. The absorption is occurring through air friction in the spirals. Analytical expectations have been explicitly explained for the Helmholtz unit and the numerical modelling have been introduced. The two microphones impedance tube method is used to extract the absorption

coefficient on a frequency range between 500 Hz and 3500 Hz. Standard deviation over a set of three measurements allowed to validate the accuracy and repeatability of the results. The dependency of the 3D printed processes has been discussed and was neglected for a first shape response study. For further process optimisations, this source of error should be taken into account. The micro-helix design has a very good mean absorption over frequencies while the two other designs need to be tuned at a specific resonant frequency. Some distortions and shifts are visible on the Helmholtz unit experiment. Each behaviour can be tuned to answer a specific application. This diversity of absorption patterns increases the number of available absorption solutions. Further investigations could be carried out on each design to identify the relevant parameters optimizing the absorption.

9. Future work

The micro helix array coupled with an air chamber is the most promising design in term of mean sound absorption. A further study could be realised to optimise its performance based on its geometry (see Fig.11).

It can be expected that the higher the array, the more the wave will have time to be attenuated by friction through thermal processes. The effect of the spacing between each helix could be investigated.

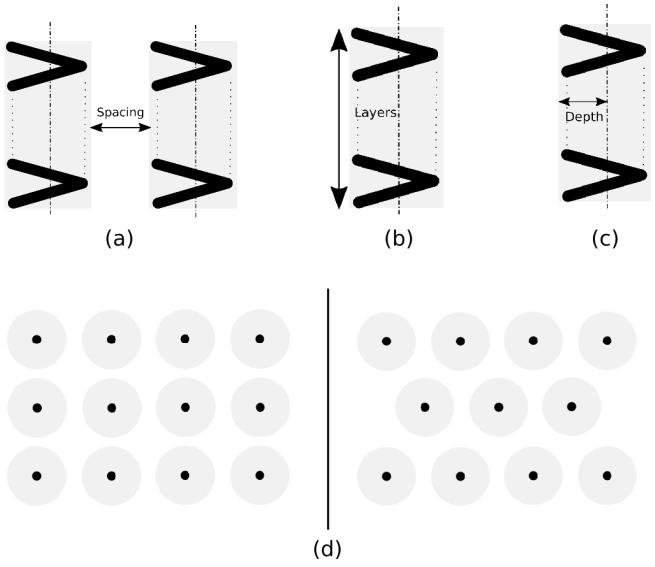

Figure 11: Geometry parameters of the micro helix array : (a) Helix spacing, (b) Number of layers, (c) Helix depth , (d) In-line / Staggered array

With the same approach, we can expect that an increase in the spacing will lead to a decrease in air pressure along the helix so less air friction. By reducing and compacting the helix, we expect to obtain better sound absorption. In the same scope, a staggered array could be printed and compare to an in-line one with similar helix geometry. If the "packing factor" of the array being is increased, we expect the same conclusion as the helix spacing.

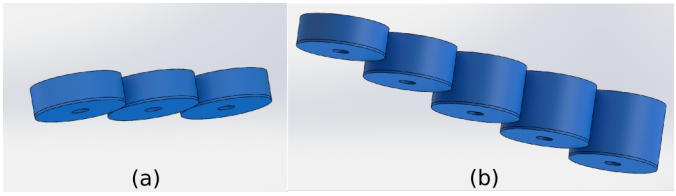

Figure 12: Split-ring neck design: (a) Linear distribution, (b) Rainbow distribution

By crossing all the results, an optimal set of parameters could be concluded. Maximum geometric values from which the phenomenon will disappear could also be deduced from the measurements.

The split-ring neck design allows reducing the transmission of a narrow range of frequencies while having a low effect in the other regions of the spectrum. The initial linear distribution can be replaced by a rainbow distribution. By modifying the dimensions of the split-ring, other peaks of absorption can be obtained other the spectrum. Depending on the applications, an array of these rings should be able to absorb the sound in some local frequencies while keeping the other part of the spectrum almost unchanged.

Acknowledgements

This work was partially funded through the AERIALIST project no: 723367 EU H2020-EU.3.4. Societal Challenges Smart, Green And Integrated Transport.

References

[1] N. Engheta (Ed.), Metamaterials: physics and engineering explorations, IEEE Press [u.a.], Piscataway, NJ, 2006, oCLC: 255422935.
[2] J. C. Bose, On the Rotation of Plane of Polarisation of Electric Waves by a Twisted Structure, Proceedings of the Royal Society of London 6 (1898) 146–152.
[3] W. Kock, Path-Length Microwave Lenses, Proceedings of the IRE 37 (8) (1949) 852–855. doi:10.1109/JRPROC.1949.229682.
[4] C. F. Bohren, R. Luebbers, H. S. Langdon, F. Hunsberger, Microwave-absorbing chiral composites: Is chirality essential or accidental?, Applied Optics 31 (30) (1992) 6403. doi:10.1364/AO.31.006403.
[5] J. Cloete, S. Kuehl, M. Bingle, The absorption of electromagnetic waves at microwave frequencies by synthetic chiral and racemic materials, International Journal of Applied Electromagnetics and Mechanics 9 (2) (1998) 103–114. doi:10.3233/JAEM-1998-108.
[6] C. Brewitt-Taylor, Fundamental limitation on the performance of chiral radar absorbing materials, Bianisotropics (2000) 27–29.
[7] R. V. Craster (Ed.), Acoustic metamaterials: negative refraction, imaging, lensing and cloaking, no. 166 in Springer series in materials science, Springer, Dordrecht, 2013, oCLC: 815367245.
[8] Z. Liu, Locally Resonant Sonic Materials, Science 289 (5485) (2000) 1734–1736. doi:10.1126/science.289.5485.1734.
[9] B. Assouar, M. Oudich, X. Zhou, Acoustic metamaterials for sound mitigation, Comptes Rendus Physique 17 (5) (2016) 524–532. doi:10.1016/j.crhy.2016.02.002.
[10] M. Han, Sound reduction by a helmholtz resonator 110.
[11] H. M. Dai, K. M. Ho, Z. Yang, P. Sheng, Non-periodic locally resonant sonic materials (2007) 8.
[12] N. Gao, H. Hou, Sound absorption characteristic of micro-helix metamaterial by 3d printing, Theoretical and Applied Mechanics Letters 8 (2) (2018) 63–67. doi:10.1016/j.taml.2018.02.001.

[13] W. Huang, H. Zhang, D. J. Inman, J. Qiu, C. E. Cesnik, H. Ji, Low reflection effect by 3d printed functionally graded acoustic black holes, Journal of Sound and Vibration 450 (2019) 96–108. doi:10.1016/j.jsv.2019.02.043.

[14] R. Vdovin, T. Tomilina, V. Smelov, M. Laktionova, Implementation of the Additive PolyJet Technology to the Development and Fabricating the Samples of the Acoustic Metamaterials, Procedia Engineering 176 (2017) 595–599. doi:10.1016/j.proeng.2017.02.302.

[15] M. Yuan, F. Yang, Z. Pang, Deep subwavelength split ring neck acoustic resonator, Results in Physics 13 (2019) 102322. doi:10.1016/j.rinp.2019.102322.

[16] J. Kennedy, L. Flanagan, L. Dowling, G. J. Bennett, H. Rice, D. Trimble, The Influence of Additive Manufacturing Processes on the Performance of a Periodic Acoustic Metamaterial, International Journal of Polymer Science 2019 (2019) 1–11. doi:10.1155/2019/7029143.

[17] C. Field, F. Fricke, Theory and applications of quarter-wave resonators: A prelude to their use for attenuating noise entering buildings through ventilation openings, Applied Acoustics 53 (1-3) (1998) 117–132. doi:10.1016/S0003-682X(97)00035-2.

[18] J. Y. Chung, D. A. Blaser, Transfer function method of measuring in-duct acoustic properties. I. Theory, The Journal of the Acoustical Society of America 68 (3) (1980) 907–913. doi:10.1121/1.384778.

[19] T. Schultz, M. Sheplak, L. N. Cattafesta, Uncertainty analysis of the two-microphone method, Journal of Sound and Vibration 304 (1-2) (2007) 91–109. doi:10.1016/j.jsv.2007.02.015.

Appendix A.

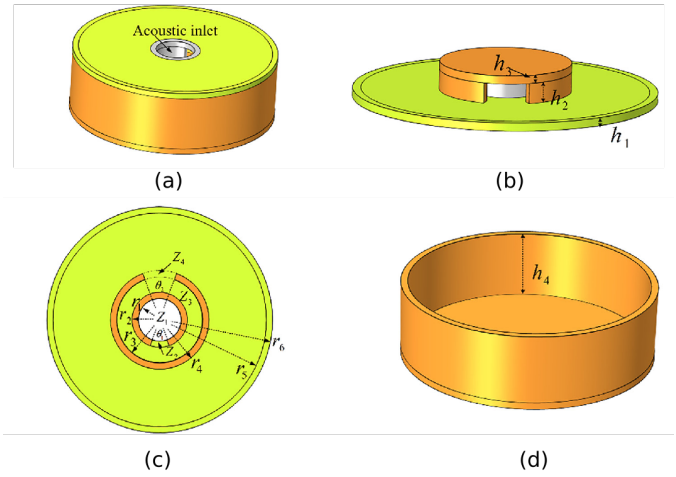

Figure A.13: Details of the split ring neck geometry [15]:
(a) Overall structure, (b) Split ring neck and upper cap,
(c) Cross section view of the split ring neck and upper cap, (d) Sound cavity

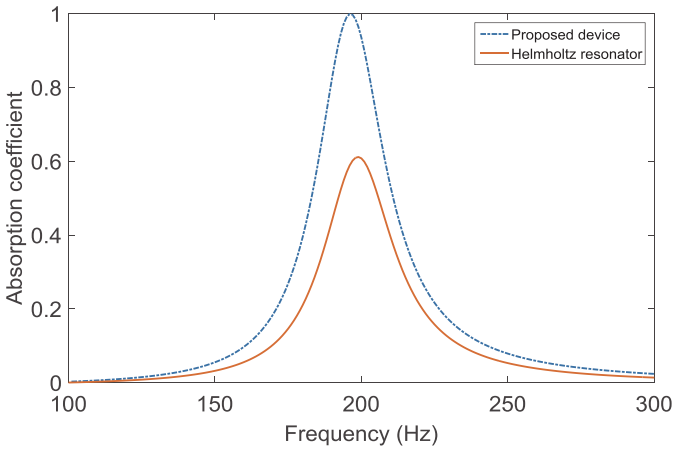

Figure A.14: Theoretical response of the split ring neck resonator compared to a frequency equivalent Helmholtz resonator

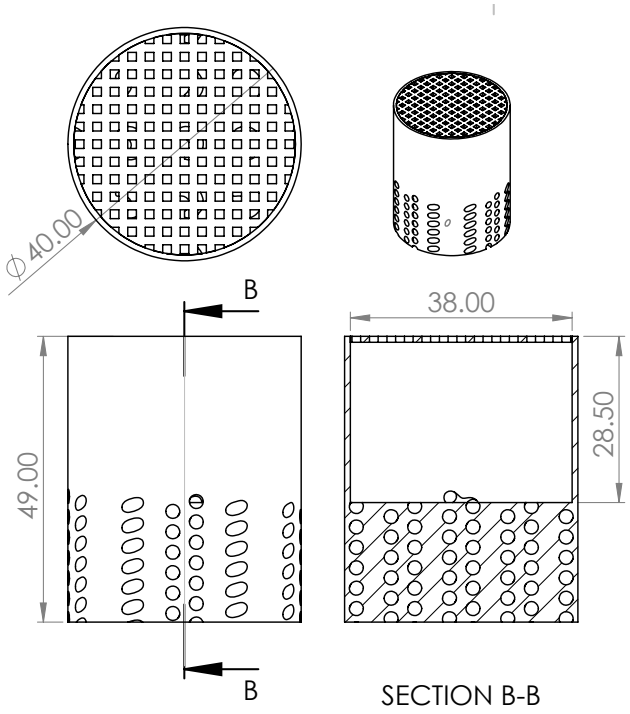

Figure A.15: Top, side and cross section views of the helix air cavity metamaterial

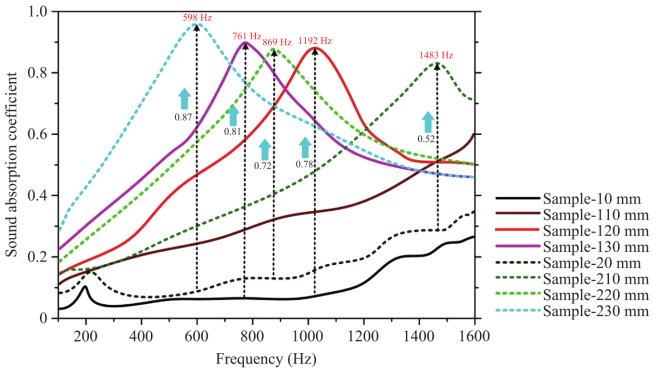

Figure A.16: Absorption depending on the helix screw pitch by Gao *et al.* [12]

View publication stats